Journal for ImmunoTherapy of Cancer

Angiotensin receptor blocker attacks armored and cold tumors and boosts immune checkpoint blockade

Jie Mei ,[1,2] Jiahui Chu,[1,2] Kai Yang,[1,2] Zhiwen Luo,[3] Jiayue Yang,[4] Junying Xu,[5] Qing Li,[6] Yan Zhang ,[7,8] Qinglin Zhang,[9] Mengyun Wan,[10] Ningyi Xue,[2,11] Junli Ding,[5] Yichao Zhu,[10] Yun Cai,[12] Yongmei Yin[1,13]

To cite: Mei J, Chu J, Yang K, *et al*. Angiotensin receptor blocker attacks armored and cold tumors and boosts immune checkpoint blockade. *Journal for ImmunoTherapy of Cancer* 2024;**12**:e009327. doi:10.1136/jitc-2024-009327

► Additional supplemental material is published online only. To view, please visit the journal online (https://doi.org/10.1136/jitc-2024-009327).

JM, JC, KY and ZL contributed equally.

JD, YZ, YC and YY are joint senior authors.

Accepted 23 August 2024

Check for updates

© Author(s) (or their employer(s)) 2024. Re-use permitted under CC BY-NC. No commercial re-use. See rights and permissions. Published by BMJ.

For numbered affiliations see end of article.

Correspondence to
Dr Yongmei Yin; ymyin@njmu.edu.cn

Dr Yun Cai; kellie_cai@163.com

Professor Yichao Zhu; zhuyichao@njmu.edu.cn

Dr Junli Ding; dingjunliletters@163.com

ABSTRACT

Background Immune checkpoint blockade (ICB) has made remarkable achievements, but newly identified armored and cold tumors cannot respond to ICB therapy. The high prevalence of concomitant medications has huge impact on immunotherapeutic responses, but the clinical effects on the therapeutic outcome of armored and cold tumors are still unclear.

Methods In this research, using large-scale transcriptomics datasets, the expression and potential biological functions of angiotensin II receptor 1 (AGTR1), the target of angiotensin receptor blocker (ARB), were investigated. Next, the roles of ARB in tumor cells and tumor microenvironment cells were defined by a series of in vitro and in vivo assays. In addition, the clinical impacts of ARB on ICB therapy were assessed by multicenter cohorts and meta-analysis.

Results AGTR1 was overexpressed in armored and cold tumors and associated with poor response to ICB therapy. ARB, the inhibitor for AGTR1, only suppressed the aggressiveness of tumor cells with high AGTR1 expression, which accounted for a very small proportion. Further analysis revealed that AGTR1 was always highly expressed in cancer-associated fibroblasts (CAFs) and ARB inhibited type I collagen expression in CAFs by suppressing the RhoA-YAP axis. Moreover, ARB could also drastically reverse the phenotype of armored and cold to soft and hot in vivo, leading to a higher response to ICB therapy. In addition, both our in-house cohorts and meta-analysis further supported the idea that ARB can significantly enhance ICB efficacy.

Conclusion Overall, we identify AGTR1 as a novel target in armored and cold tumors and demonstrate the improved therapeutic efficacy of ICB in combination with ARB. These findings could provide novel clinical insight into how to treat patients with refractory armored and cold tumors.

WHAT IS ALREADY KNOWN ON THIS TOPIC

⇒ Collagen deposition in extracellular matrix is the main physical barrier hindering immune cell infiltration. We previously identified a refractory armored and cold subtype featured by high collagen deposition and low immune cell infiltration. However, effective antitumor therapies for armored and cold tumors are largely unknown.

WHAT THIS STUDY ADDS

⇒ We systematically screened potential drug targets of concomitant medications that were differentially expressed in armored and cold tumors and identified that angiotensin II receptor 1 (AGTR1) as a biomarker and therapeutic target for armored and cold tumors, which was highly expressed in cancer-associated fibroblasts. Accordingly, the AGTR1 inhibitor angiotensin receptor blocker (ARB) suppressed the collagen synthesis and ARB use could significantly enhance the response to ICB in patients with cancer.

HOW THIS STUDY MIGHT AFFECT RESEARCH, PRACTICE OR POLICY

⇒ Our findings provide novel clinical insight for the control of armored and cold tumors using a combination therapy of ARB and immune checkpoint blockade, contributing to enhancing the management of immunotherapy in patients with cancer.

BACKGROUND

As an emerging therapy for cancer, immune checkpoint blockade (ICB) has made remarkable achievements, but not all patients with advanced tumors respond to ICB therapy. Therefore, the population of potential beneficiaries should be screened before receiving ICB treatment. The tumor microenvironment (TME) is a highly complicated system that mainly consists of immune cells, stromal cells, and extracellular matrix (ECM) molecules within the tumor, which affects multiple hallmarks of cancer.[1] The TME has great impacts on tumor progression, and remodeling of the TME has emerged as a strategy to facilitate the development of cancer therapies.[2] As the most notable features of cellular components and molecules, various immune cells and collagens remarkably affect antitumor immunity.[3–6] Collagens are synthesized by cancer-associated fibroblasts (CAFs), and collagen deposition is the most important physical factor hindering immune cell

infiltration.[7 8] In our previous study, we developed a pan-cancer immuno-collagenic subtyping strategy to stratify patients according to collagen deposition and immune activity and identified a refractory cancer subtype, which was defined as armored and cold tumors accompanied by high collagen activity and low immune infiltration.[9 10] Accordingly, effective antitumor therapies are still unavailable for armored and cold tumors.

Patients with cancer are frequently prescribed multiple medications for pre-existing comorbidities or side effects from antitumor therapy.[11 12] Polypharmacy is common among patients with cancer with one study reporting polypharmacy in up to 84% of patients.[13] Considering the high prevalence of concomitant medications and the potential interactions with ICB, an increasing number of studies have focused on the potential effects of common medications on the response to ICB. Several investigators have found that patients taking concomitant medications like proton pump inhibitors, antibiotics, or steroids while receiving immunotherapy had less clinical benefit, suggesting notable impacts of concomitant medications on ICB efficacy.[14] In our previous report, we revealed the significance of cholesterol synthesis in non-small cell lung cancer (NSCLC) and demonstrated the improved therapeutic efficacy of ICB in combination with statins.[15] Thus, we speculated that concomitant medications may affect the therapeutic outcome of armored and cold tumors.

In the current research, based on our established immuno-collagenic subtyping strategy, we systematically screened potential drug targets of concomitant medications that were differentially expressed in armored and cold tumors and identified that angiotensin II receptor 1 (AGTR1) was highly expressed in armored and cold tumors. Further analysis revealed that AGTR1 was positively expressed in CAFs and the AGTR1 inhibitor angiotensin receptor blocker (ARB) suppressed the RhoA/YAP axis to decrease type I collagen expression. Moreover, both our in-house data and meta-analysis implicate that ARB use could significantly enhance the response to ICB. Overall, these results may provide novel clinical insight for the control of armored and cold tumors using a combination therapy of ARB and ICB.

METHODS

Acquisition of transcriptomics datasets

Transcriptome profiles and clinical information of 31 solid cancer types in The Cancer Genome Atlas (TCGA) datasets were obtained from the University of California Santa Cruz Xena (https://xenabrowser.net/datapages/). Samples with overall survival (OS) were selected for further analysis. A panel of public immunotherapy datasets, including the GSE173839 dataset,[16] the GSE194040 dataset,[17] and the GSE135222 dataset,[18] comprising transcriptome data from patients with cancer receiving ICB, were downloaded from the Gene Expression Omnibus database. The transcriptome data and clinical information of the IMvigor210 cohort were obtained from the official website (http://research-pub.gene.com/IMvigor210CoreBiologies/).[19] The GSE173839 and the GSE194040 datasets were directly merged due to the same sequencing platform and processing method for these two datasets. The gene expression profile of cell lines was downloaded from the Cancer Cell Line Encyclopedia (CCLE) database.[20] Tissues with at least five sample collection sites were reserved. Cell lines with AGTR1>1 were defined as AGTR1$^+$ samples. The single-cell RNA sequencing (scRNA-seq) data of a total of 10 breast cancer (BRCA) samples was described in our previous study.[21] The annotations of the used datasets are summarized in online supplemental table S1.

Single-cell RNA sequencing analysis

For alignment and preprocessing procedures of the scRNA-seq dataset, Cell Ranger V.3.0.2 was used to perform sample demultiplexing, barcode processing, and generating gene count data for each cell based on the hg38/GRCh38 reference genome. The R package "Seurat"[22] was used for all additional analysis. First, we removed the low-quality cells in which the expression of mitochondrial genes was greater than 10% or with detected genes less than 200 or greater than 5000. Then, the R package "harmony"[23] was used to minimize the technical batch effects among individuals and experiments and subsequently integrate the scRNA-seq datasets. The principal component analysis was first performed on the top 4000 genes with the highest variants, and then the first 30 principal components (PCs) were used to reduce the dimensionality. The shared nearest neighbor modularity optimization-based clustering algorithm was used to unsupervised these cells into many clusters with a resolution of one. t-distributed stochastic neighbor embedding (t-SNE) was used to visualize the distribution of cells in the two-dimensional space. For fibroblasts, the "RunHarmony" function was used to integrate the scRNA-seq profile of fibroblasts from different individuals. The first 20 PCs established based on the top 2000 variable genes were used to reduce the dimensionality. To explore the biological functions of AGTR1$^+$ CAFs, the "FindAllMarkers" function was used. Genes with avg_log2FC≥1, pct.1≥0.1 and $p<0.05$ were identified as AGTR1$^+$ CAFs-enriched. The R package "clusterProfiler"[24] was used to investigate the enriched biological pathways based on these genes. Biological process (BP) among Gene Ontology (GO)[25] terms were identified with a strict cut-off of $p<0.05$. Based on the percentage of AGTR1$^+$ cells in CAFs, we divided the patients into AGTR1-positive and AGTR1-negative groups based on 10%. To assess the functional status of CD8$^+$ T cells at the single cell level, the "AddModuleScore" function was used to estimate the activated scores of each cell by using these markers: IL2, GZMA, GNLY, PRF1, GZMB, GZMK, IFNG, NKG7, and CD69.

Gene set enrichment analysis

To explore the special functions of CAFs, the gene set enrichment analysis (GSEA) was performed using the

"GSEA" function in the "clusterProfiler" package in terms of gene signatures. The collagen signature was obtained from our previous research.[10] To define the metastasis-associated fibroblasts (MAFs) signature, the transcriptional omics of fibroblasts associated with metastasis were obtained from the GSE145428 dataset.[26] Then, the "limma" package was used to perform differential expression analysis between CAFs and MAFs. Genes with FC≥1.5 and adjusted p<0.05 were identified as the gene signature of MAFs. The YAP conserved signature was obtained from published research.[27]

Reagents and antibodies

Losartan (catalog HY-17512) and YAP agonist XMU-MP-1 (catalog HY-100526) were purchased from MedChemExpress (Shanghai, China). ELISA kits for IL-2 (catalog RK04123) and TNF-α (catalog RK00030) were purchased from Abclonal (Wuhan, China). The PD-1 in vivo mAb (catalog BE0273) was purchased from BioXCell (Lebanon, USA), and the CD8 in vivo mAb (catalog A2102) was purchased from Selleck (Shanghai, China). TRITC Phalloidin (catalog 40734ES75) was purchased from Yeasen (Shanghai, China). RhoA G-LISA activation assay kit (catalog BK124) was purchased from Cytoskeleton (Denver, USA). ImmunoCult human CD3/CD28 T cell activator (catalog 10971) was purchased from STEMCELL Technologies (Vancouver, Canada). Antibodies used in the study are exhibited in online supplemental table S2.

Clinical samples

Four independent cohorts were included in this study. Cohort 1 contained 63 paraffin-embedded bladder cancer (BLCA) samples and 16 para-tumor samples (catalog HBlaU079Su01). Cohort 2 contained 75 paraffin-embedded BRCA samples (catalog HBreD075Bc01). Cohorts 1–2 were obtained from Outdo BioTech (Shanghai, China). Cohort 3 was an immunotherapy cohort and included 105 NSCLC patients recruited from The Affiliated Wuxi People's Hospital of Nanjing Medical University receiving ICB therapy from January 2019 to December 2022. Five paraffin-embedded tumor samples from patients with ARB use obtained via biopsy before immunotherapy were retrospectively collected. As a control, another five samples from patients with no ARB use were also randomly collected. Paraffin-embedded samples were used for immunohistochemistry (IHC), multiplexed IHC (mIHC), and histochemistry staining. Cohort 4 was also an immunotherapy cohort and included 165 NSCLC patients recruited from The First Affiliated Hospital of Nanjing Medical University receiving ICB therapy from January 2019 to December 2022. The therapeutic response was evaluated according to the RECIST V.1.1 criteria, which were demarcated into complete response, partial response, stable disease, and progressive disease. The ARB medication history was obtained by reviewing the medical records. The detailed clinic-pathological features and immunotherapy information can be found in online supplemental table S3.

IHC, mIHC, and histochemistry staining

Human paraffin-embedded cancer tissues underwent IHC staining of PD-L1, mIHC staining of AGTR1, CD8, and α-SMA, Masson staining, and HE staining. Standard operating procedures were employed for IHC, mIHC, and HE staining. A ready-to-use anti-PD-L1 antibody (catalog GT2280, GeneTech, Shanghai, China) was used for IHC staining. The visualization of IHC staining was carried out using EnVision FLEX$^+$ (catalog K8009, Dako, Copenhagen, Denmark). Think color staining kit (catalog FH34020R, FreeThinking, Nanjing, China) was used for mIHC staining following the manufacturer's instructions. The primary antibodies used for mIHC staining were as follows: anti-AGTR1 (1:10000 dilution, catalog SAB3500209, Sigma), anti-CD8 (1:1000 dilution, catalog 85336, CST), and anti-α-SMA (1:2000 dilution, catalog 19245, CST). Masson's staining was conducted using the Trichrome Stain Kit (catalog FH115100, FreeThinking, Nanjing, China) following the manufacturer's instructions. PD-L1 staining was quantitatively assessed by two dependent senior pathologists based on the combined positive score (CPS), mIHC staining was evaluated using HALO software (V.3.4.2986, Indica Labs, Albuquerque, USA) to determine cells positive with various markers, and Masson staining was evaluated using HALO software to determine positive-stained area percentages.

Primary CAFs and cell lines

Primary CAFs were isolated from breast tumor tissues[28] and cultured using a primary cell culture medium (catalog CX0013, Yuchi, Shanghai, China). Primary AGTR1$^+$ CAFs were further identified by microscopic morphology, the presence of CAF-specific biomarker α-SMA, and the presence of AGTR1 (online supplemental figure S1A–C). Human cancer cell lines MDA-MB-231 (catalog KGG3220-1), NCI-H1299 (catalog KGG3216-1), HGC-27 (catalog KGG3287-1), HS578T (catalog KGG3375-1), and mouse cancer cell line 4T1 (catalog KGG2224-1) were purchased from KeyGEN (Nanjing, China). NCI-H1299 and HGC-27, cells were cultured in RPMI-1640 media, and MDA-MB-231, HS578T, and 4T1 cells were cultured in DMEM media. All media were added with 10% FBS at 37°C with 5% CO_2. All human cell lines were authenticated using short tandem repeat profiling and all assays were conducted with mycoplasma-free. For in vitro assays, cells were treated with 10 µM losartan and/or 1 µM XMU-MP-1.

In vitro assays for cellular functions

In order to assess cell proliferation levels, suspended cancer cells were seeded into a 96-well plate at a cell density of 5×10^3 cells/mL (100 µL/well) and incubated at 37°C. Afterward, 10 µL of CCK-8 reagent (catalog KGA9305, KeyGEN, Nanjing, China) was added to each well and the plate was incubated for 2 hours. The optical

density of each well was then measured at 450 nm using a microplate reader. In addition, cancer cells were seeded in six-well plates at a density of 500 cells per well and cultured at 37°C for 1–2 weeks. At the end of the incubation, colonies were stained with crystal violet solution for 30 min. Wells were rinsed with water followed by air drying and the colonies were counted. Each measurement was performed in triplicate. In order to assess cell migration and invasion levels, Transwell chambers were used; with or without Matrigel (Corning) coating depending on the desired assay. Cancer cells (5×10^4) in 200 µL of serum-free medium were seeded in the upper chamber while 600 µL of medium containing 10% FBS was added to the lower chamber. In addition, CAFs (5×10^4) were also used for cell migration analysis. After 24 hours, the cells that had migrated/invaded the lower surface of the membrane were observed and counted. In order to assess cell apoptosis levels, the apoptosis of cancer cells was analyzed by Annexin V-FITC/PI Kit (Cat. KGA1102, KeyGEN, Nanjing, China) according to the manufacturer's instructions. Annexin V positive and PI negative cells were early apoptotic cells.

Quantitative real-time PCR

The total RNA of cells was extracted using Trizol reagent (catalog KGF5101, KeyGEN, Nanjing, Nanjing). The primers for COL1A1 and GAPDH mRNA reverse transcription were synthesized in KeyGEN (Nanjing, China). Quantitative real-time PCR (qRT-PCR) was performed using the One-Step TB GreenTM PrimeScriptTM RT-PCR Kit II (SYBR Green) (catalog RR086B, TaKaRa, Kyoto, Japan). Primers used for gene amplification were as follows: COL1A1: (forward) 5'-GCAACATGGAGACTGG TGAGA-3' and (reverse) 5'-GGGGTTCTTGCTGATG TACCA-3'; GAPDH (forward) 5'-AGATCATCAGCA ATGCCTCCT-3' and (reverse) 5'-TGAGTCCTTCCA CGATACCAA-3'.

Western blotting analysis

CAFs were maintained in six-well plates. The total proteins of cells were harvested using a lysis buffer. Then, SDS-PAGE and Western blotting analysis were conducted according to standardized protocols. The primary antibodies used as follows: AGTR1 (1:1000 dilution, catalog SAB3500209, Sigma-Aldrich), COL1A1 (1:1000 dilution, catalog A24112, Abclonal, Wuhan, China), YAP (1:1000 dilution, catalog 13584–1-AP, ProteinTech), p-YAP (1:1000 dilution, catalog 13008, Cell Signaling Technology), RhoA (1:1000 dilution, catalog 10749-1-AP, ProteinTech), and GAPDH (1:2000 dilution, catalog 60004-1-Ig, ProteinTech). Protein levels were standardized to GAPDH.

Immunofluorescence and actin cytoskeleton staining

The expression levels of COL1A1 and YAP were assessed using immunofluorescence assay according to standardized protocols.[29] The primary antibodies used were as follows: COL1A1 (1:200 dilution, catalog, 67288-1-Ig, ProteinTech) and YAP (1:200 dilution, catalog 13584-1-AP, ProteinTech). In addition, CAFs were also subjected to actin cytoskeleton staining using TRITC Phalloidin (catalog 40734ES75, Yeasen). The detailed protocol was described previously.[29] The stained cells were visualized using a fluorescence microscope.

RhoA GTPase activation assays

Total protein lysates extracted from CAFs were turned to measure RhoA activity by using the RhoA G-LISA activation assay kit (catalog BK124) purchased from Cytoskeleton (Denver, USA). RhoA activation was described as previously.[30]

In vitro cytotoxicity assay

Peripheral blood monouclear cells (PBMC) were collected from a healthy control. The $CD8^+$ T cells were isolated using Dynabeads human CD8 selection Kit (catalog 11333D, Invitrogen) and cultured in ImmunoCult-XF T cell expansion medium (catalog 10981, STEMCELL Technologies). ImmunoCult human CD3/CD28 T cell activator (catalog 10971, STEMCELL Technologies) was used to activate T cells, and then T cells were transferred into a 24-well plate and co-cultured with CAFs at an effector-to-target ratio of 5:1 at 37°C for 48 hours. T cells were submitted for PCR array (catalog WC-MRNA0138-H, WcGene Biotech) and flow cytometry analysis to detect the activated marker GZMB. The levels of cytokines TNF-α and IL-2 in the supernatant were detected using the ELISA assay.

Animal models

Female Balb/c mice (5–6 weeks old) obtained from the Zhejiang Vital River Laboratory Animal Technology were housed in specific pathogen-free facilities at 22°C±2°C under 12-hour light/dark cycles. To test the effect of losartan on the blood pressure of Balb/c mice, losartan was administrated orally to Balb/c mice with 10 mg/kg, 20 mg/kg, and 30 mg/kg for 1 week, and the blood pressure was detected by the BP-2000 animal blood pressure analysis system (Visitech System). Mouse cancer models were established by subcutaneously injecting approximately 5×10^6 4T1 cells into each Balb/c mouse. Tumor size was monitored using calipers, and tumor volume (V) was calculated using the formula $V=(\text{length}\times\text{width}^2)/2$. On tumors reaching an average size of approximately 50 mm^3, tumor-bearing mice were randomly assigned to groups and administrated with losartan therapy immediately. Mouse cancer models were randomly divided into three groups in the first round and four groups in the second round. Three groups included control, losartan-treated, and losartan-treated and CD8-deleted groups, and four groups included control, losartan-treated, anti-PD-1-treated, and losartan and anti-PD-1-treated groups. The control group received oral administration of phosphate buffered saline (PBS). Losartan therapy was oral administration of losartan (catalog. HY-17512, MedChemExpress) at 10 mg/kg daily. Anti-PD-1 therapy group was

intraperitoneally injected with anti-mouse PD-1 antibody (catalog BE0273, clone 29F.1A12, BioXCell) at 200 µg/mouse three times a week. The CD8-deleted group was intraperitoneally injected with anti-mouse CD8 antibody (catalog A2102, clone 2.43, Selleck) at 100 µg/mouse two times a week. The course of mAb therapies (anti-CD8 and anti-PD-1) was started 2 weeks after the first losartan treatment and maintained for 2 weeks. Mice were euthanized using carbon dioxide (Euthanex Chamber) about another week after the last mAb therapies (online supplemental figure S2). The tumors were removed from the unconscious animals, which were subsequently documented and weighed.

Peripheral blood of mice was collected to detect liver and kidney functions using the automatic biochemical analyzer (catalog Chemray 240, Rayto, Shenzhen, China). The removed main organs, including heart, liver, and kidney, were submitted for HE staining, and the removed tumors were submitted for HE, Masson, and IHC staining of CD8 (1:1000 dilution, catalog ab209775, Abcam), anti-AGTR1 (1:10 000 dilution, catalog SAB3500209, Sigma), and Ki67 (1:1000 dilution, catalog ab15580, Abcam), and flow cytometry. The harvested tumors were mechanically dissociated into 1 mm^3 fragments and then incubated with lysis buffer (RPMI-1640+Collagenase IV 1 mg/mL, DNase I 0.5 mg/mL) to obtain single cell suspensions. Mouse TILs were incubated with CD16/CD32 to block Fc receptors and then stained with Fixable Viability Dye eFluor 780, fluorescence-conjugated anti-CD45, anti-CD3e, anti-CD8a, CD11b, and Gr-1 antibodies (online supplemental table S2). Stained samples were analyzed with BD FACSymphony A5 SORP (BD Biosciences, Franklin, USA).

Meta-analysis

The databases of Web of Science (https://www.webofscience.com/wos/woscc/basic-search) and PubMed (https://pubmed.ncbi.nlm.nih.gov) were systematically searched up until January 10, 2024. Two authors independently reviewed the titles and abstracts of these publications according to the inclusion and exclusion criteria, and then the full text was screened for further confirmation. Finally, 4 studies involving 1268 participants in total were included in our meta-analysis.[31–34] In addition, an in-house cohort with 270 participants was also included after quality evaluation. The following characteristics of the studies were recorded in online supplemental table S4: first author's name, publication year, design, country, cancer type, and case number. We performed an additional meta-analysis on the association between the use of ARBs in patients with cancer receiving ICB therapy and OS. HRs and their 95% CIs were recorded to calculate pooled HR using the software Stata V.15.0.

Statistical analysis

Statistical analyses and figure presentations were conducted using R language V.4.0.2 and GraphPad Prism V.6.0. All R packages used in this study are summarized in online supplemental table S5. Group differences were assessed using the Student's t-test or Mann-Whitney test for two groups while a one-way analysis of variance or the Kruskal-Wallis test with multiple comparisons was used for multiple groups. Categorical variables were assessed using the χ^2 test or Fisher's exact probability test. Pearson's or Spearman's correlation tests were employed to evaluate correlations between variables. Prognostic values of categorical variables were assessed via log-rank test and Cox regression analysis. A $p<0.05$ was considered statistically significant for all analyses.

RESULTS

AGTR1 is overexpressed in armored and cold tumors and predicts resistance to ICB therapy

Based on our established subtypes,[10] we aimed to investigate the potential therapeutic targets in terms of concomitant medications. Common concomitant medications and their targets, including statins (HMGCR), cyclooxygenase inhibitors (PTGS1, PTGS2), ACE inhibitors (ACEI), ARB (AGTR1), β-blockers (ADRB1, ADRB2, ADRB3), melbines (PPKAA1, PPKAA2), opioids (OPRM1), and proton pump inhibitors (ATP4A, ATP4B, ATP12A), were collected and their expression across various immunocollagenic subtypes was assessed in the TCGA-BLCA cohort, one of the most suitable tumor type to apply this classification (figure 1A). We found that PTGS1, PTGS2, AGTR1, and ADRB3 were highly expressed in armored-cold tumors (figure 1B, online supplemental figure S3). Next, we also checked the expression of these four targets in other solid tumor types, and the results showed that the overexpression of AGTR1 in armored-cold tumors was conserved (online supplemental figure S4). We, therefore, chose AGTR1 for further study. Overexpression of AGTR1 was associated with poor prognosis in the TCGA-BLCA cohorts (figure 1C). The protein expression of AGTR1 was also checked using in-house cohorts. Similar to the previous results,[10] PD-L1 and CD8 were lowly expressed in armored and cold tumors, and AGTR1 was highly expressed in armored and cold tumors in the in-house BLCA cohort (figure 1D–G). In addition, in the in-house breast cancer (BRCA) cohort, CD8 was lowly expressed in armored and cold tumors, and AGTR1 was highly expressed in armored and cold tumors (online supplemental figure S5A–C). Moreover, high expression of AGTR1 predicted poor prognosis in the in-house BLCA cohort (figure 1H). Moreover, AGTR1 was associated with poor immunotherapeutic response and worse prognosis in three independent immunotherapy cohorts (figure 1I–K). Overall, the integrated analysis revealed that AGTR1 was overexpressed in armored and cold tumors and predicted poor immunotherapeutic response.

ARB has no antitumor effect on most tumor cells due to the low level of AGTR1 expression

Considering the clinical significance of AGTR1 in cancerous diseases, we examined the expression and

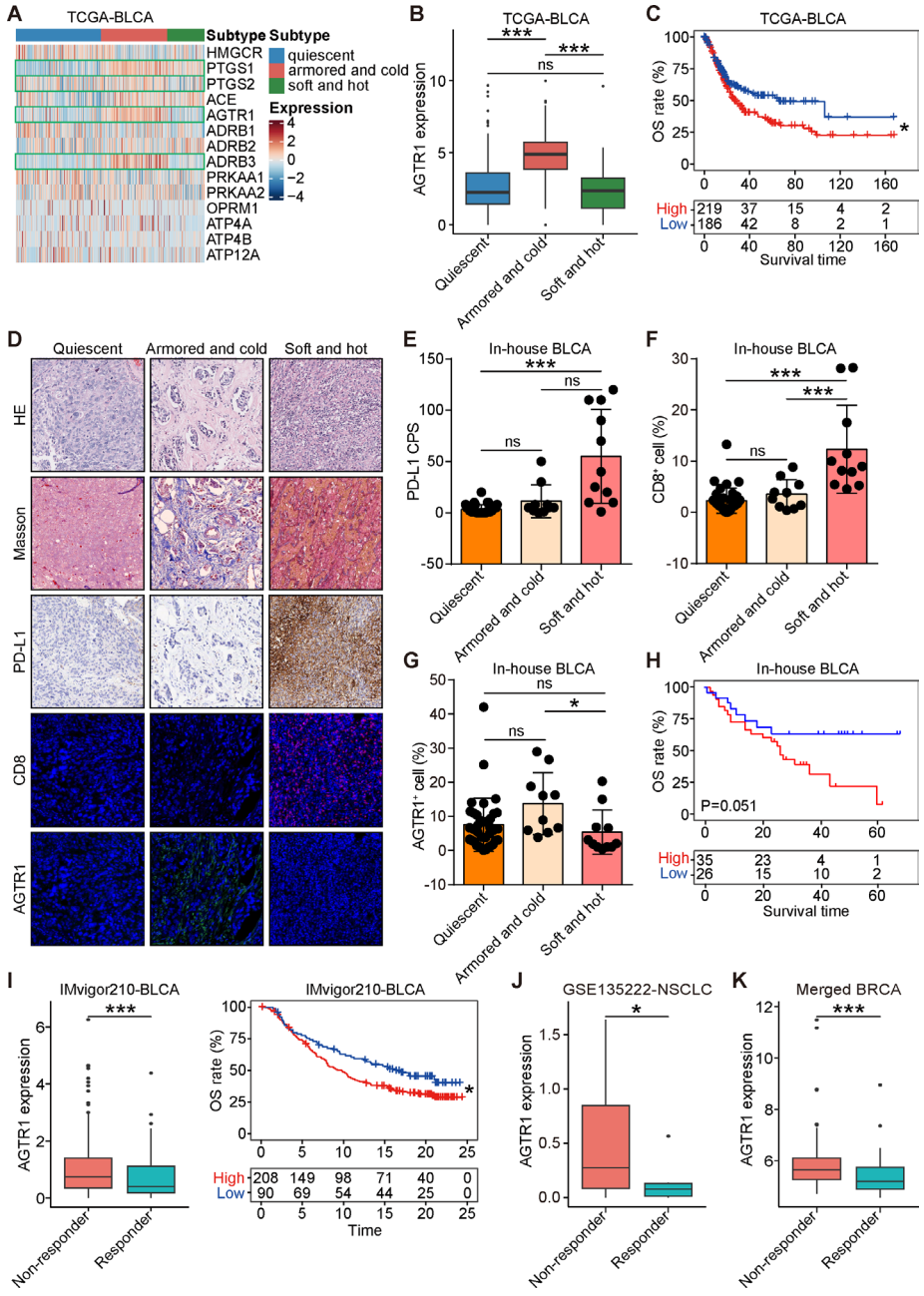

Figure 1 AGTR1 highly expresses in armored and cold tumors and predicts low response to immune checkpoint blockade (ICB) therapy. (A) Heatmap showing the targets expression of concomitant medications in the three immuno-collagenic subtypes in the TCGA-BLCA cohort. (B) Boxplot showing high expression of AGTR1 in armored and cold tumors in the TCGA-BLCA cohort. Horizontal lines in the boxplots represent the median value, and the lower and upper hinges correspond to the first and third quartiles, respectively. Significance was calculated using the ANOVA with Tukey's multiple-comparison test. ns, non-significance, ***p<0.001. (C) Prognostic value of AGTR1 in the TCGA-BLCA cohort. Subgroups for survival analysis were divided by the best cut-off point. Significance was calculated using the log-rank test. *p<0.05. (D) Representative images uncovering stromal and immune markers in the three immuno-collagenic subtypes in the in-house BLCA cohort. Staining data of HE, Masson, and PD-L1 IHC from our previous study [10] was used as controls. A total of 61 samples were analyzed due to 2 samples losses during multiple staining procedures. (E–G) Expression of PD-L1, CD8, and AGTR1 in the three immuno-collagenic subtypes in the in-house BLCA cohort. Data was presented as mean±SD. Significance was calculated using the Kruskal-Wallis test with the Dunn's multiple-comparison test for (E). Significance was calculated using the ANOVA with Tukey's multiple-comparison test for (F and G). ns, non-significance, *p<0.05, ***p<0.001. (H) Prognostic value of AGTR1 in the in-house BLCA cohort. Subgroups for survival analysis were divided by the value of 5%. Significance was calculated using the log-rank test. (I) Predictive value and prognostic value of AGTR1 in the IMvigor210 cohort. Subgroups for survival analysis were divided by the best cut-off point. Significance was calculated using the Student t-test (left) and the log-rank test (right). *p<0.05, ***p<0.001. (J, K) Predictive value of AGTR1 in the GSE135222 and the merged BRCA cohorts. Significance was calculated using the Mann-Whitney test (J) and the Student's t-test (K). *p<0.05, ***p<0.001. ANOVA, analysis of variance; BLCA, bladder cancer; TCGA, The Cancer Genome Atlas.

cellular role of AGTR1 in cancer cells. The results from the CCLE database showed that the positive rates of tumor cells derived from different organs were notably various, and malignant fibroblasts expressed the highest AGTR1 (figure 2A), suggesting fibroblasts were the primary target cells of AGTR1 expression. Next, we used an in-house scRNA-seq dataset[21] to analyze the expression pattern of AGTR1 in various cell types in cancer tissues. In this dataset, we found that AGTR1 was primarily expressed in CAFs (figure 2B,C). In addition, four tumor cell lines and the primary CAFs were subjected to Western blotting analysis and the results revealed that HS578T cells and CAFs expressed higher AGTR1 (figure 2D). Also, the colocation of AGTR1 and α-SMA in the in-house BLCA and BRCA cohorts further supported the above point (figure 2E, online supplemental figure S6A, B). The cellular effects of AGTR1 inhibitor, losartan, on tumor cells with various AGTR1 expressions were examined. Notably, losartan did not affect cell proliferation, apoptosis, migration, and invasion of tumor cells with low AGTR1 expression, including MDA-MB-231, H1299, and HGC27 cells (figure 2F–I, online supplemental figure S7A–F), but notably inhibited the malignant capabilities of HS578T cells, which expressed high AGTR1 (figure 2F–I, online supplemental figure S7A). Taken together, AGTR1 inhibitor ARB only inhibited tumor cells with high AGTR1 expression, but the positive rate of AGTR1 in solid tumors was low. Thus, we suspected the main functions of ARB in cancer were dependent on its effects on CAFs.

ARB inhibits collagen expression and CAF migration by suppressing the RhoA-YAP axis

Given that the main function of CAFs was the synthesis of collagen and the abundance of type I collagen was the highest among all collagen subtypes in cancer tissues,[7 35] we aimed to check the effects of ARB on collagen expression in CAFs. AGTR1 expression was positive in all 10 cancer samples, suggesting that the functions of AGTR1 were conserved (figure 3A,B). To determine the functions of AGTR1 in CAFs, we performed GO-BP analysis between $AGTR1^+$ and $AGTR1^-$ CAFs. AGTR1 expression was significantly associated with ECM organization (figure 3C). Evidence from the clinical samples also revealed that the number of $AGTR1^+$ cells was positively correlated with collagen area (online supplemental figure S8A–D). In addition, the GSEA analysis revealed AGTR1 was related to collagen signature and migration signature (figure 3D–F). Next, in vitro assays revealed that losartan significantly downregulated type I collagen expression and migration of CAFs (figure 3G–I). Furthermore, the remodeling of microfilaments in CAFs was also blocked by losartan (figure 3J).

The mechanisms underlying ARB-mediated collagen inhibition were subsequently explored. The YAP signaling pathway has been reported to be associated with fibrosis in various disease models.[36–38] The GSEA analysis of CAFs revealed that AGTR1 was associated with the YAP conserved signature (figure 4A). Then, analysis of YAP1 expression pattern uncovered that YAP1 was mainly expressed in CAFs (figure 4B,C). Coexpression analysis of YAP1 and COL1A1 in the CAFs using our in-house scRNA-seq dataset showed that YAP1 was highly correlated with COL1A1 (figure 4D). Moreover, pan-cancer analysis of the TCGA database also supported that YAP1 was positively correlated with COL1A1 expression (figure 4E). Subsequently, in vitro assays exhibited that losartan inhibited RhoA activity and increased the phosphorylation of YAP (figure 4F,G). Immunofluorescence analysis further validated that losartan suppressed the nuclear translocation of YAP in CAFs (figure 4H). Given the notable role of YAP activity in losartan-mediated collagen inhibition, we used a YAP agonist, XMU-MP-1, to reverse the above effects. The results showed that XMU-MP-1 notably blocked losartan-mediated type I collagen inhibition (figure 4I,J). In conclusion, these results suggested that ARB decreased type I collagen expression in CAFs by inhibiting the RhoA-YAP axis (figure 4K).

ARB shapes a soft and hot TME and enhances the anti-PD-1 immunotherapy response

Collagen deposition is the most important physical factor hindering immune cell infiltration,[8] thus we suspected that the inhibition of AGTR1 may reverse collagen-mediated immune escape. Based on the percentage of $AGTR1^+$ cells in CAFs from our scRNA-seq dataset, we divided the patients into AGTR1-positive and AGTR1-negative groups based on 10% (figure 5A). We next assessed the functional status of $CD8^+$ T cells at the single cell level. The results showed that the exhausted level of $CD8^+$ T cells was increased but the cytotoxic activity of $CD8^+$ T cell was decreased in AGTR1-positive cancer samples (figure 5B). Then, the T cells was co-cultured with CAFs with or without losartan (figure 5C), and the activity level of T cells was examined by PCR array. The results showed that most activated markers were upregulated and inhibitory markers were downregulated in T cells cocultured with CAFs with losartan treatment (figure 5D,E). In addition, the level of GZMB in T cells was also checked by flow cytometry and the results showed that GZMB was highly expressed in T cells cocultured with CAFs with losartan treatment (online supplemental figure S9A, B). In addition, the level of activating inflammatory factors, including IL-2 and TNF-α, was also highly expressed in the losartan-treated cocultured medium (figure 5F). These results suggested that losartan notably suppressed CAF-mediated T cell inhibition. Moreover, evidence from the clinical samples also revealed that the number of $AGTR1^+$ cells was negatively correlated with the number of $CD8^+$ cells (figure 5G, online supplemental figure S10A–C). To assess the hypotensive of losartan in vivo, we administrated losartan to Balb/c mice with 10 mg/kg, 20 mg/kg, and 30 mg/kg for 1 week, and the results showed that losartan decreased blood pressure in a dose-dependent manner, and the dose of 10 mg/kg did not significantly affect blood pressure (online supplemental figure S11). Thus, the dose of 10 mg/kg was used for the next in vivo assays. Losartan

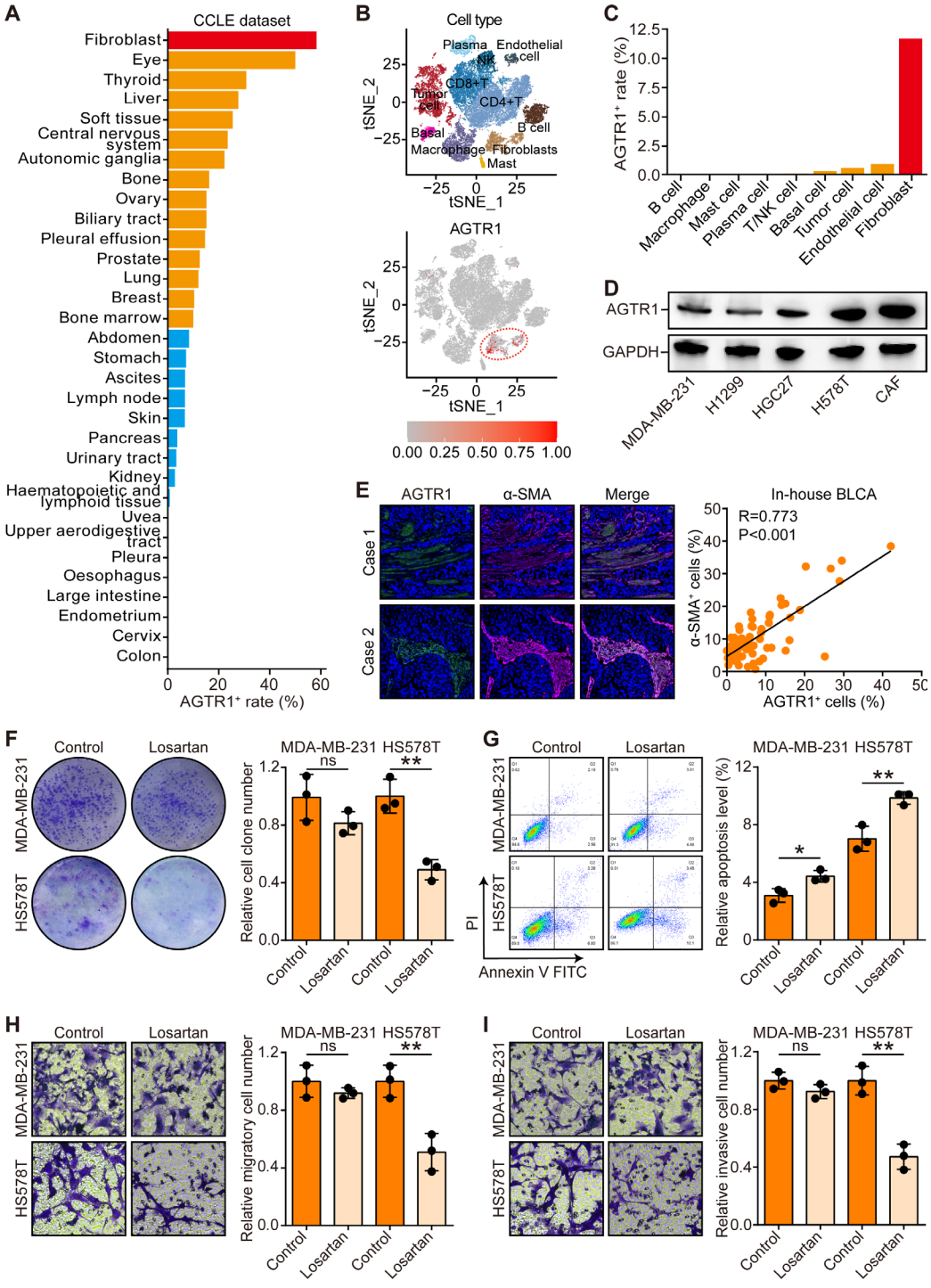

Figure 2 Angiotensin receptor blocker (ARB) suppresses the aggressiveness of tumor cells with high AGTR1 expression. (A) Positive rate of AGTR1 expression in malignant cells originated from various tissues in the Cancer Cell Line Encyclopedia (CCLE) dataset. (B) t-distributed stochastic neighbor embedding (t-SNE) visualization of cell types annotated by classical gene markers in our published cohort and expression of AGTR1 in various cell types. (C) Positive rate of AGTR1 in various cell types. (D) Expression of AGTR1 in MDA-MB-231, NCI-H1299, HGC27, H578T, and CAF cells. (E) Representative images uncovering the co-location between AGTR1 and α-SMA in the in-house BLCA cohort and quantitative analysis. Data was presented as mean±SD. Significance was calculated with the Pearson test. (F) Proliferation ability of MDA-MB-231 and HS578T cells in control and losartan-treated groups was assessed by colony formation assay. The experiment was performed three times. Data was presented as mean±SD. Significance was calculated with the Student's t-test. ns, non-significance, **p<0.01. (G) Apoptosis level of MDA-MB-231 and HS578T cells in control and losartan-treated groups was assessed by flow cytometry assay. Data was presented as mean±SD. Significance was calculated with the Student's t-test. *p<0.05, **p<0.01. (H, I) Migration and invasion ability of MDA-MB-231 and HS578T cells in control and losartan-treated groups were assessed by Boyden chamber assay. Data was presented as mean±SD. Significance was calculated with the Student's t-test test. ns, non-significance, **p<0.01.

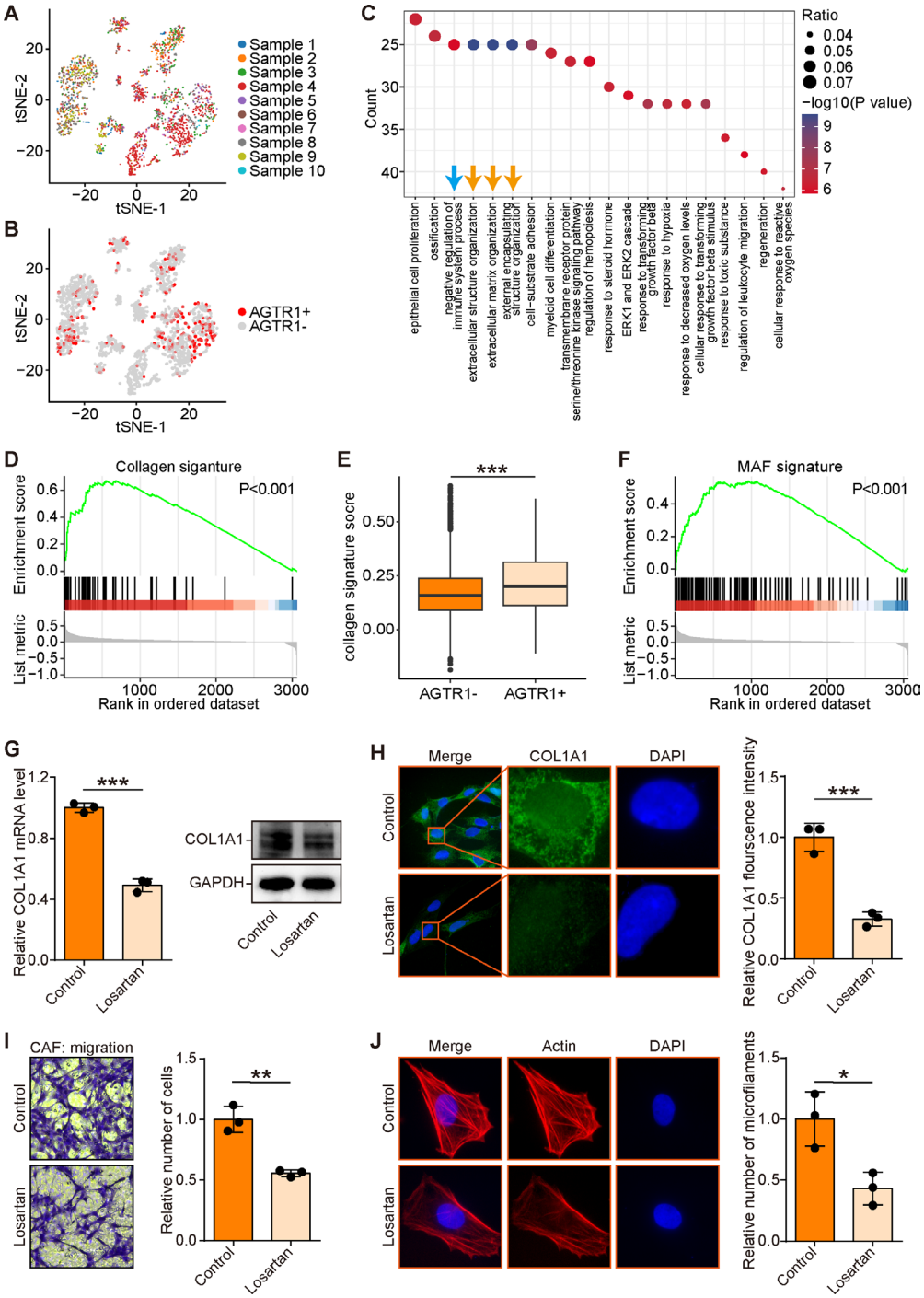

Figure 3 Angiotensin receptor blocker (ARB) inhibits collagen expression and migration of cancer-associated fibroblasts (CAFs). (A) t-distributed stochastic neighbor embedding (t-SNE) visualization of 2081 single cells passed quality controls, colored by 10 BRCA patients in our published cohort. (B) Expression pattern of AGTR1 in fibroblasts overlaid on t-SNE. Red points represent the cells with AGTR1 expression. (C) Functional enrichment analysis of genes highly expressed on AGTR1^{+} fibroblasts in the term of Gene Ontology biologocal process. (D) GSEA of collagen signature between fibroblasts with positive and negative AGTR1. (E) Difference in collagen signature score in fibroblasts with positive and negative AGTR1. Data was presented as mean±SD. Significance was calculated with the Student's t-test. (F) GSEA of metastasis-associated fibroblast (MAF) signature between fibroblasts with positive and negative AGTR1. (G) Expression of COL1A1 in control and losartan-treated CAFs was assessed by qPCR and Western blotting assays. Data was presented as mean±SD. Significance was calculated with the Student's t-test. ***p<0.001. (H) Expression of COL1A1 in control and losartan-treated CAFs was assessed by immunofluorescence assay. Data was presented as mean±SD. Significance was calculated with the Student's t-test. ***p<0.001. (I) Migration ability of control and losartan-treated CAFs was assessed by Boyden chamber assay. Data was presented as mean±SD. Significance was calculated with the Student's t-test test. **p<0.01. (J) The formation of microfilament in control and losartan-treated CAFs was assessed by immunofluorescence assay. Data was presented as mean±SD. Significance was calculated with the Student's t-test test. *p<0.05. BRCA, breast cancer; GSEA: gene set enrichment analysis.

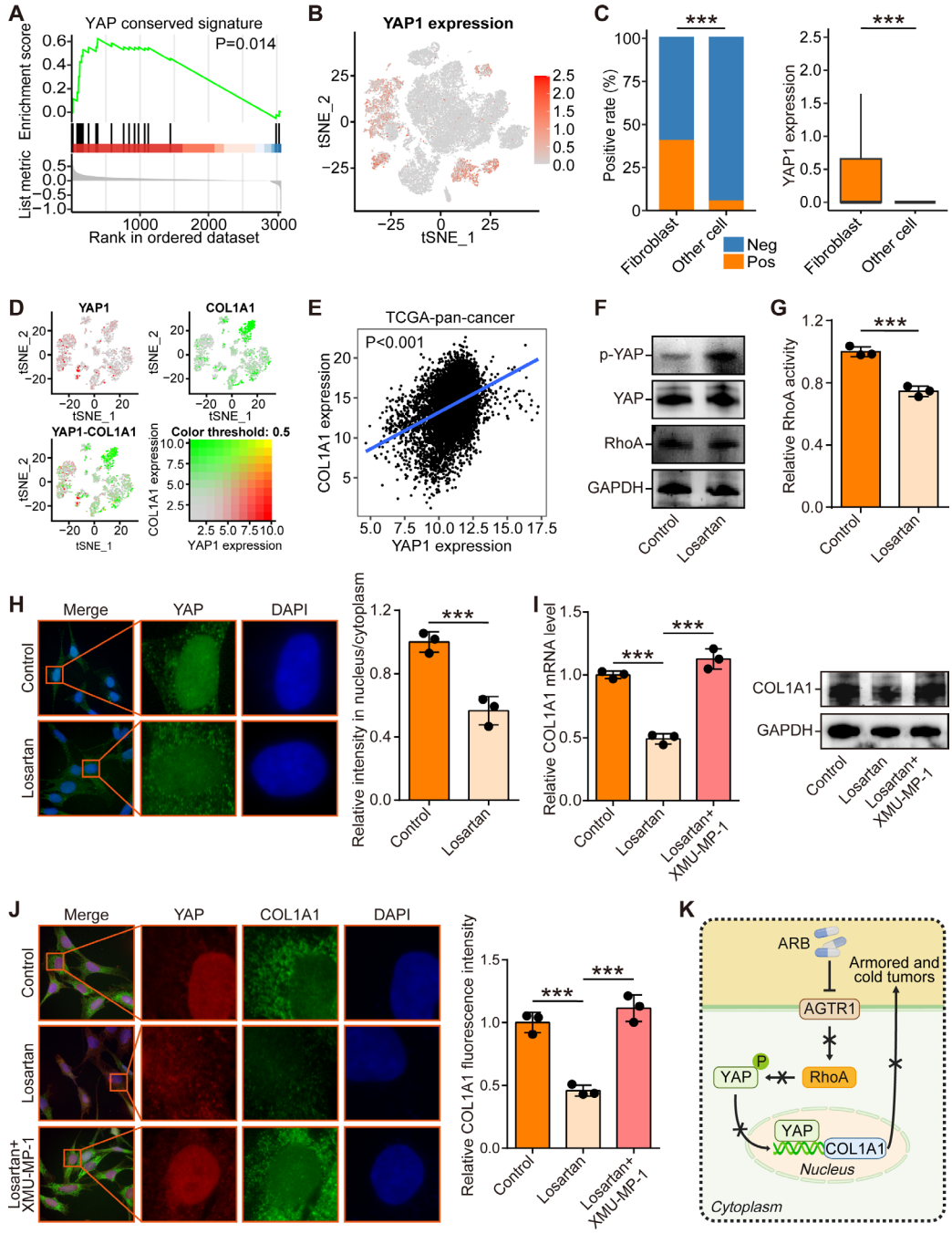

Figure 4 Angiotensin receptor blocker (ARB) inhibits collagen expression via suppressing the RhoA-YAP axis. (A) GSEA of YAP conserved signature between fibroblasts with positive and negative AGTR1. (B) Expression of YAP1 in various cell types in our published cohort. (C) Positive rate (left) and expression level (right) of YAP1 in fibroblasts and non-fibroblasts. Significance was calculated with the Pearson's χ^2 test and Student's t-test test. ***p<0.001. (D) Expression of YAP1 (gray to red) and COL1A1 (gray to green) on overlaid on the t-distributed stochastic neighbor embedding (t-SNE) representation. (E) Correlation between YAP1 and COL1A1 in the The Cancer Genome Atlas (TCGA) pan-cancer dataset. Significance was calculated with the Pearson test. (F) The expression of RhoA, YAP and phosphor-YAP in control and losartan-treated CAFs was assessed by Western blotting assay. (G) The level of RhoA activity in control and losartan-treated CAFs was assessed by GLISA assay. Data was presented as mean±SD. Significance was calculated with the Student's t-test test. ***: p<0.001. (H) The location of YAP in control and losartan-treated CAFs was assessed by immunofluorescence assay. Data was presented as mean±SD. Significance was calculated with the Student's t-test test. ***p<0.001. (I) Expression of COL1A1 in control, losartan-treated, and losartan and XMU-MP-1 co-treated CAFs was assessed by qPCR and Western blotting assays. Data was presented as mean±SD. Significance was calculated using the ANOVA with Tukey's multiple-comparison test. ***p<0.001. (J) Expression of COL1A1 in control, losartan-treated, and losartan and XMU-MP-1 co-treated CAFs was assessed by immunofluorescence assays. Data was presented as mean±SD. Significance was calculated using the ANOVA with Tukey's multiple-comparison test. ***p<0.001. (K) Schematic overview of mechanism underlying losartan-mediated regulation of type I collagen. ANOVA, analysis of variance; CAFs, cancer-associated fibroblasts.

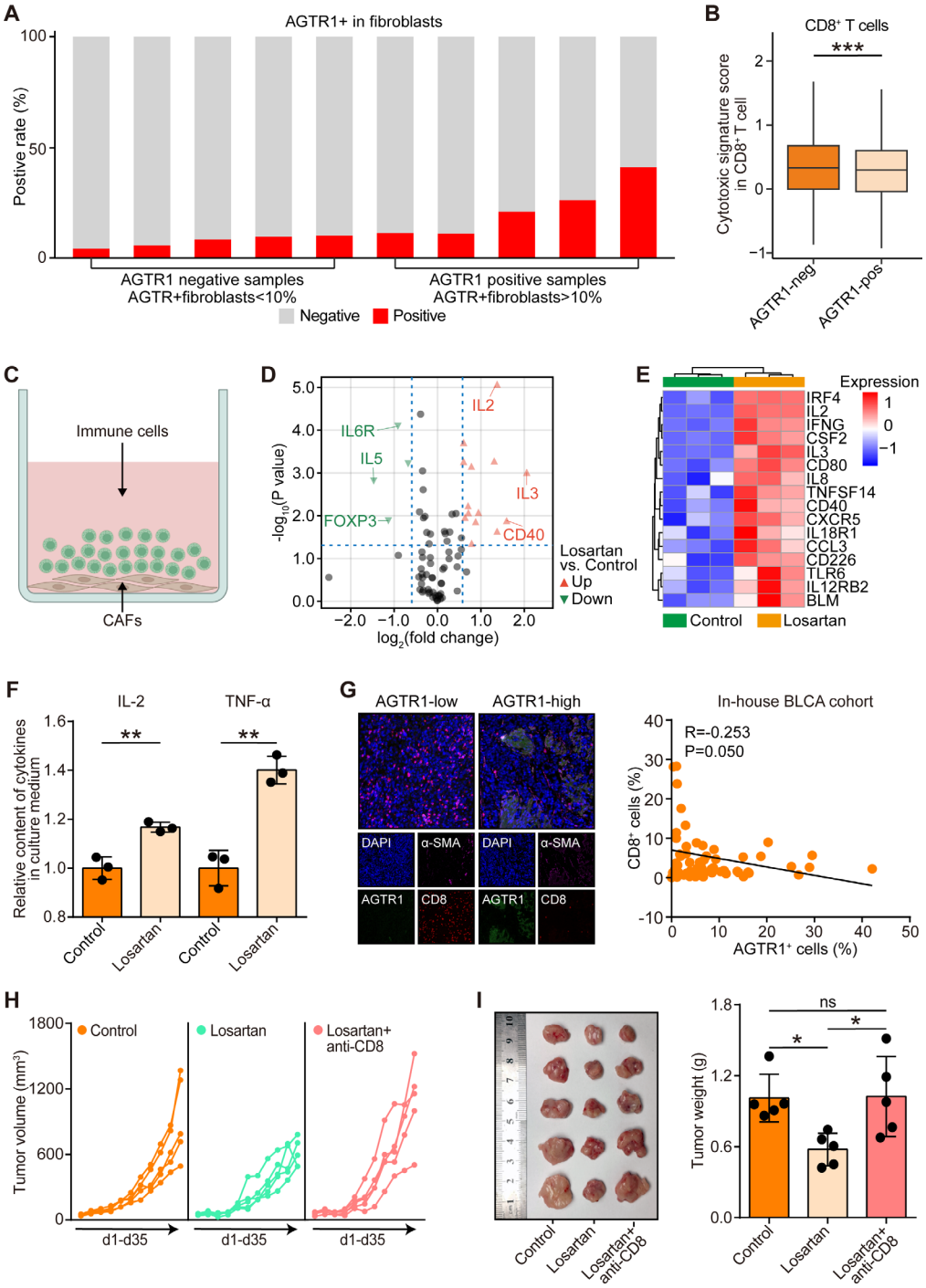

Figure 5 ARB reverses CAFs-mediated T cell inhibition and exerts immune-dependent tumor suppressive role. (A) The positive rate of AGTR1 in CAFs in 10 BRCA samples in our published cohort. Based on the percentage of AGTR1$^+$ cells in CAFs, BRCA patients were divided into AGTR1-positive and AGTR1-negative groups based on 10%. (B) Boxplot showing exhausted and cytotoxic signature scores in CD8$^+$ T cells in AGTR1-positive and AGTR1-negative groups. Horizontal lines in the boxplots represent the median value, and the lower and upper hinges correspond to the first and third quartiles, respectively. Significance was calculated using the Student's t-test. ***p<0.001. (C) Schematic protocol of co-culture of CAFs and T cells. (D, E) Differentially expressed genes and expression of activated markers in T cells identified by T cell activation PCR array. (F) Relative content of cytokines in supernatant from the co-culture system was assessed by ELISA assay. Data was presented as mean±SD. Significance was calculated with the Student's t-test. **p<0.01. (G) Representative images uncovering CD8$^+$ T cell infiltration in samples with low and high AGTR1 expression in the in-house BLCA cohort and quantitative analysis. Significance was calculated using the Pearson test. (H) Tumor growth curve of mice treated with PBS, losartan, and losartan+anti-CD8 antibody. (I) Representative images showing the tumors harvested from mice bearing Lewis cells treated with PBS, losartan, and losartan+anti-CD8 antibody, and weight of the harvested tumors. Data was presented as mean±SD. Significance was calculated with one-way ANOVA with Tukey's multiple-comparison test. ns, non-significance, *p<0.05. BRCA, breast cancer; ANOVA, analysis of variance; ARB, angiotensin receptor blocker; BLCA, bladder cancer; CAFs, cancer-associated fibroblasts.

did not affect the proliferation of 4T1 tumor cells in vitro (online supplemental figure S12A, B), but notably inhibited tumor growth in vivo (figure 5H,I). In addition, the losartan-mediated tumor inhibition could be reversed by CD8 deletion (figure 5H,I), suggesting the antitumor effect of losartan was dependent on tumor immunity.

Furthermore, we administrated losartan and/or anti-PD-1 antibody to Balb/c mice harboring 4T1 cells. Both tumor volume (figure 6A) and tumor weight (figure 6B) were decreased remarkably in mice that received the combined therapy. In addition, the histological staining of the heart, the liver, and the kidney as well as biochemical analysis of liver and renal functions revealed a good tolerance of combination therapy (figure 6C, online supplemental figure S13A–C). Histological analysis was conducted to examine the levels of collagen, AGTR1, CD8, and Ki67. The result showed that losartan and combined therapy significantly inhibited collagen deposition and AGTR1 expression, increased cytotoxic T cell infiltration and also inhibited the expression of Ki67 in tumor cells (figure 6D). Moreover, flow cytometric analysis uncovered notable elevations in the quantity of total cytotoxic T cells and decreased myeloid-derived suppressor cells (MDSC) quantity in the tumors in which both therapies were administered (figure 6E,F). In summary, these findings suggest that ARB shapes a soft and hot TME and raises the efficacy of PD-L1 blockade in vivo.

ARB use enhances the response to ICB therapy and prolongs the survival of patients with cancer

Given the strong association between AGTR1 and ARB and immuno-collagenic in silico, in vitro, and in vivo, we next examined the effect of ARB use on the clinical outcome of NSCLC. We collected two in-house cohorts containing 105 and 165 NSCLC patients receiving anti-PD-1/PD-L1 immunotherapy. We evaluated the therapeutic response according to the RECIST V.1.1 criteria, and the survival data and HE staining image were also obtained (figure 7A). In addition, a total of 10 FFPE samples from 5 ARB users and 5 ARB non-users were obtained (figure 7A). Results indicate that ARB use significantly improved the OS of NSCLC patients in the two dependent cohorts (figure 7B,C). In addition, the tumor samples obtained from ARB users exhibited low expression of stromal markers (collagen, α-SMA, and AGTR1) and high expression of immune markers (CD8 and PD-L1) (figure 7D). Furthermore, the integrated analysis of the two in-house cohorts supported that ARB use was associated with low fibrosis levels and high immune cell infiltration (figure 7E). Also, ARB use significantly enhanced the therapeutic response to immunotherapy and improved the OS of NSCLC patients in the integrated cohort (figure 7F,G). More importantly, the meta-analysis further confirmed that ARB use was notably related to the improvement of OS in patients with cancer receiving immunotherapy (figure 7H). Overall, such findings suggest that the use of ARB was an auxiliary strategy to reverse the armored and cold tumors and raise the response to ICB therapy.

DISCUSSION

Hypertension is recognized as one of the most common comorbidities in patients with cancer.[39] However, the role of pre-existing hypertension in patients with cancer under treatment has not been thoroughly studied.[39] ARB is the most widely used antihypertension drug.[40] Evidence from clinical models reveals that ARB use is associated with decreased risks of death in several cancer types, suggesting the benefits of ARB in the management of human cancer.[41–43] One early study confirmed that the tumor-suppressive role of ARB in cancer cells was dependent on AGTR1 expression.[44] However, protein expression data from the Human Protein Atlas database reveals that AGTR1 is negative in almost all tumor cells but only positive in tumor stromal cells in several samples.[45 46] Thus, the mechanisms underlying the tumor-suppressive effects of ARB need to be further investigated.

The effects of ARB on tumor progression are contradictory in previous reports.[47–51] Based on large-scale transcriptomics data and validation using paraffin-embedded cancer tissues, we examined the expression patterns of AGTR1 and revealed that AGTR1 was negatively expressed in most cancer cells but highly expressed in a subset of CAFs. Losartan could not exert a tumor-suppressive role in AGTR1-negative tumor cells, but inhibited AGTR1-positve tumor cells. As revealed by a previous study, losartan only inhibited cell proliferation of breast cancer cells with high AGTR1 expression, such as BT549 and Hs578T cells, but not affect cell proliferation of cells with low AGTR1 expression, including SKBR-3, MDA-MB-231, BT20, DU145 cells.[44] Given the low positive rate of AGTR1 in tumor cells, we firmly believed that the effects of ARB on tumor cells themselves were not a major factor in its control of tumor progression and drug response.

It has been well acknowledged that the renin–angiotensin–aldosterone system plays a significant role in liver, cardiac, and renal fibrosis.[52] Recently, AGTR1, the receptor angiotensin II, is also reported to promote tumor fibrosis, and its inhibitor ARB significantly suppresses collagen I deposition.[51 53] Generally, the angiotensin II/AGTR1 axis is considered to favor tumor growth and shape the immunosuppressive TME, whereas the angiotensin-1-7/MAS signaling has opposing effects.[54 55] In this research, we reported that CAFs expressed high AGTR1 and losartan notably inhibited the migration and collagen I expression of CAFs. In addition, losartan shaped an inflamed TME and enhanced anti-PD-1 immunotherapy in the mouse armored and cold tumor model.

Although AGTR1 inhibition leads to a decrease in collagen I deposition in tumor tissues, the mechanisms are largely unclear. We investigated the potential mechanisms in this study. RhoA, which was reported to be a downstream of AGTR1,[26] was significantly inhibited by losartan. RhoA activates YAP via the polymerization of F-actin.[56 57] Notably, losartan destroyed the microfilament in CAFs and inhibited the activity of YAP. It has been known that YAP could directly and indirectly regulate type I collagen expression in various pathophysiological conditions.[58–62] We also used the

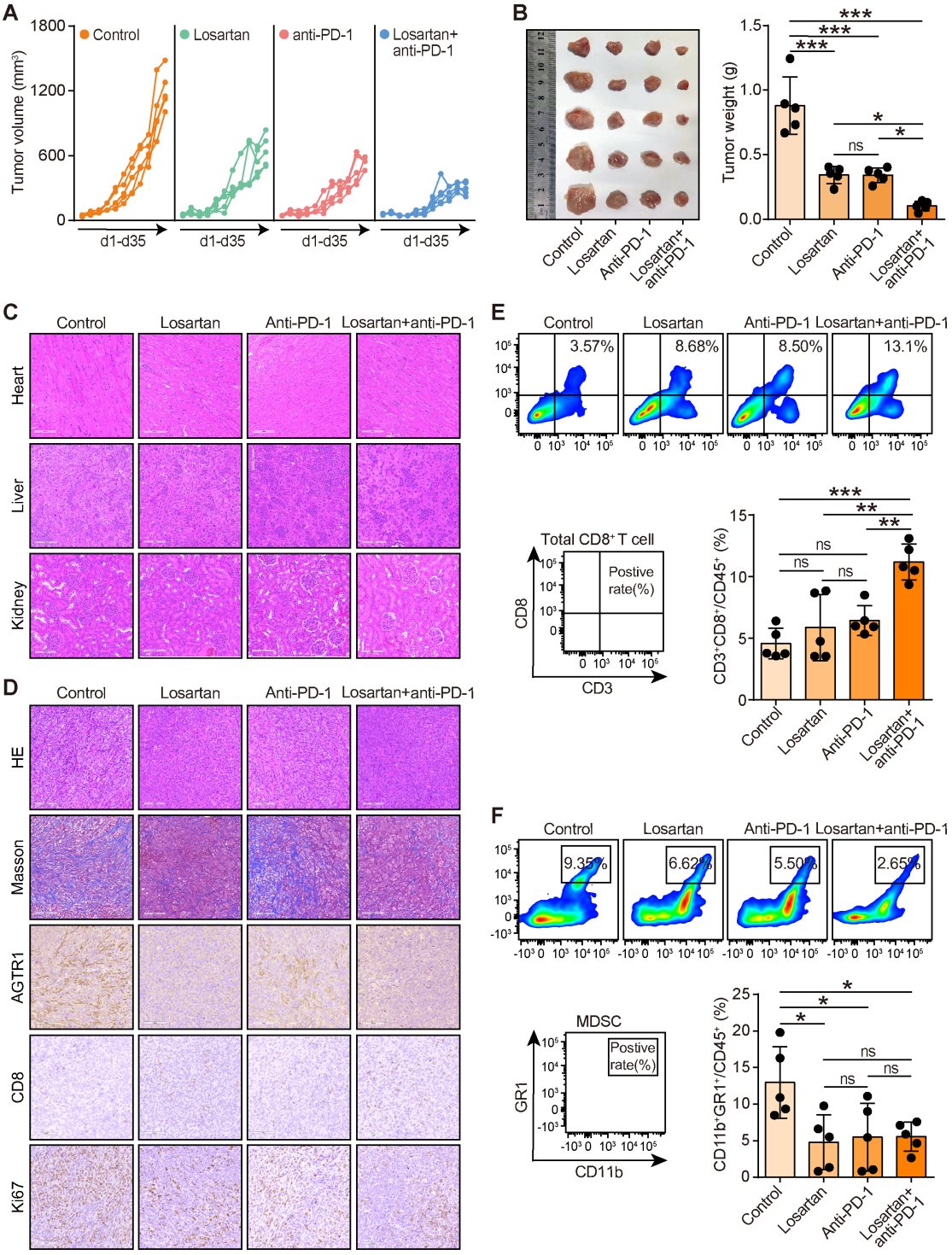

Figure 6 Angiotensin receptor blocker (ARB) shapes an inflamed tumor microenvironment (TME) and enhances immunotherapy in vivo. (A) Tumor growth curve of mice treated with PBS, losartan, anti-PD-1 antibody, and the combination. (B) Representative images showing the tumors harvested from mice bearing Lewis cells treated with PBS, losartan, anti-PD-1 antibody, and the combination, and weight of the harvested tumors. Data was presented as mean±SD. Significance was calculated with one-way ANOVA with Tukey's multiple-comparison test. ns, non-significance, *p<0.05, ***p<0.001. (C) Representative images showing structure of heart, liver, and kidney from mice in different groups. (D) Representative images showing the levels of collagen, AGTR1, CD8, and Ki67 in tumor tissues from mice in different groups. (E) Representative results of flow cytometry analysis of total $CD8^+$ T cells represented by $CD3^+CD8^+$ and quantitative analysis. Data was presented as mean±SD. Significance was calculated with one-way ANOVA with Tukey's multiple-comparison test. ns, non-significance, **p<0.01, ***p<0.001. (F) Representative results of flow cytometry analysis of myeloid-derived suppressor cells (MDSC) represented by $CD11b^+Gr\text{-}1^+$ and quantitative analysis. Data was presented as mean±SD. Significance was calculated with one-way ANOVA with Tukey's multiple-comparison test. ns, non-significance, ***p<0.001. PBS: phosphate buffer saline; ANOVA, analysis of variance.

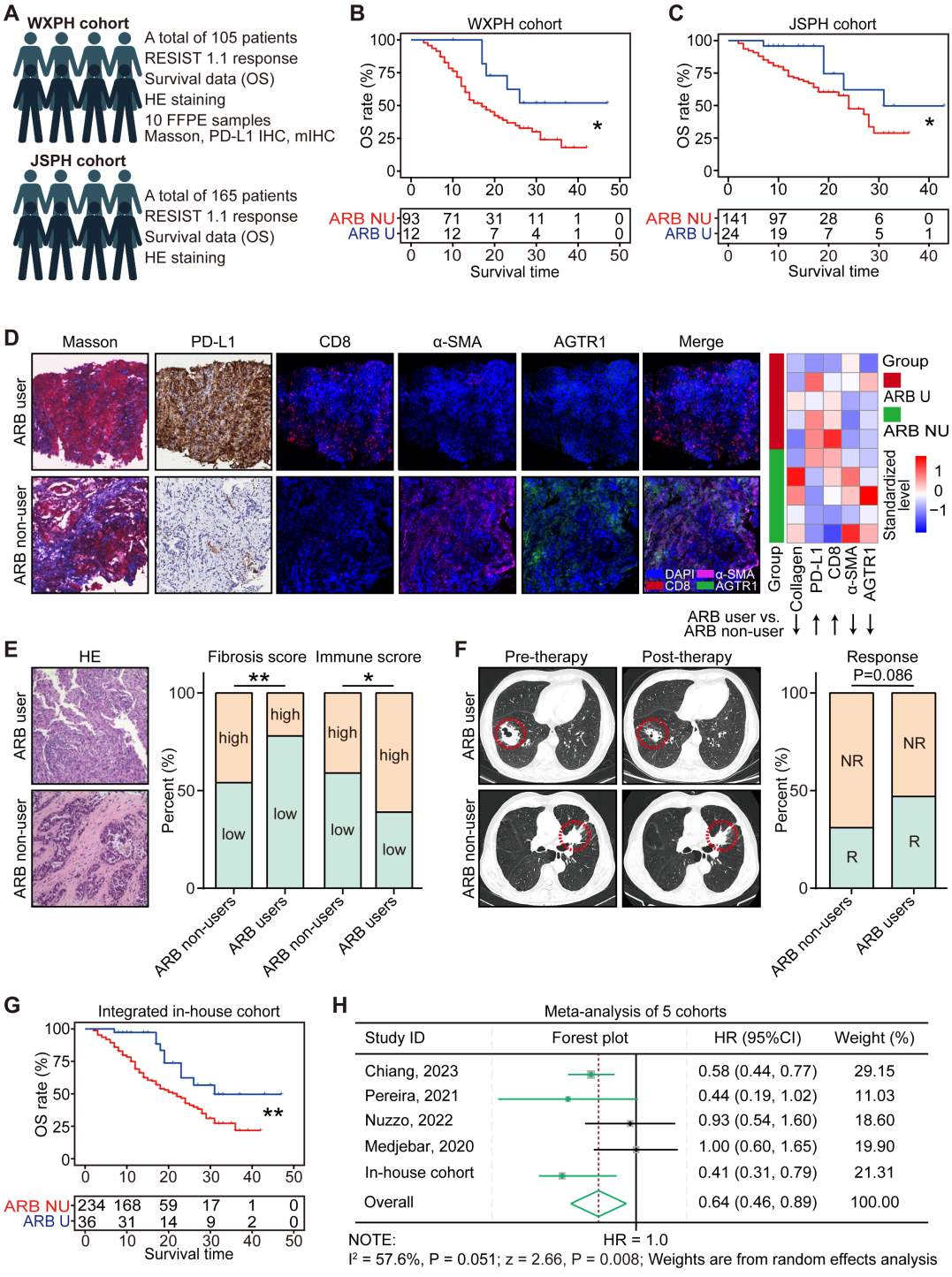

Figure 7 Angiotensin receptor blocker (ARB) use prolongs the survival of patients with cancer receiving immune checkpoint blockade (ICB) therapy. (A) Overview of the two-center immunotherapy cohort consisting of 270 patients, the HE staining images of all patients were collected. In addition, paraffin-embedded tumor samples from 10 patients obtained from ARB users and ARB non-users (5 vs 5) via biopsy before immunotherapy was subjected to mIHC, PD-L1 IHC, and Masson staining analyses. (B, C) Comparison of overall survival (OS) with log-rank test in patients with ARB use and those with never ARB use in the recruited WXPH and JSPH cohorts. *p<0.05. (D) Representative images uncovering stromal and immune markers in patients with ARB use and no ARB use and quantitative analysis. Data was presented as single value in the format of pheatmap. (E) Representative HE staining images from patients with ARB use and no ARB use, and comparison of collagen score and immune score in patients with ARB use and no ARB use in the in-house cohort. Significance was calculated with the Pearson's χ^2 test. *p<0.05, **p<0.01. (F) Representative CT images from patients with ARB use and no ARB use revealing various immunotherapeutic responses, and comparison of immunotherapeutic response in patients with ARB use and no ARB use in the in-house cohort. Significance was calculated with the Pearson's χ^2 test. (G) Comparison of OS with log-rank test in patients with ARB use and those with never ARB use in the integrated cohort. **p<0.01. (H) Pooled analysis comparing OS in patients with ARB use and those with no ARB use.

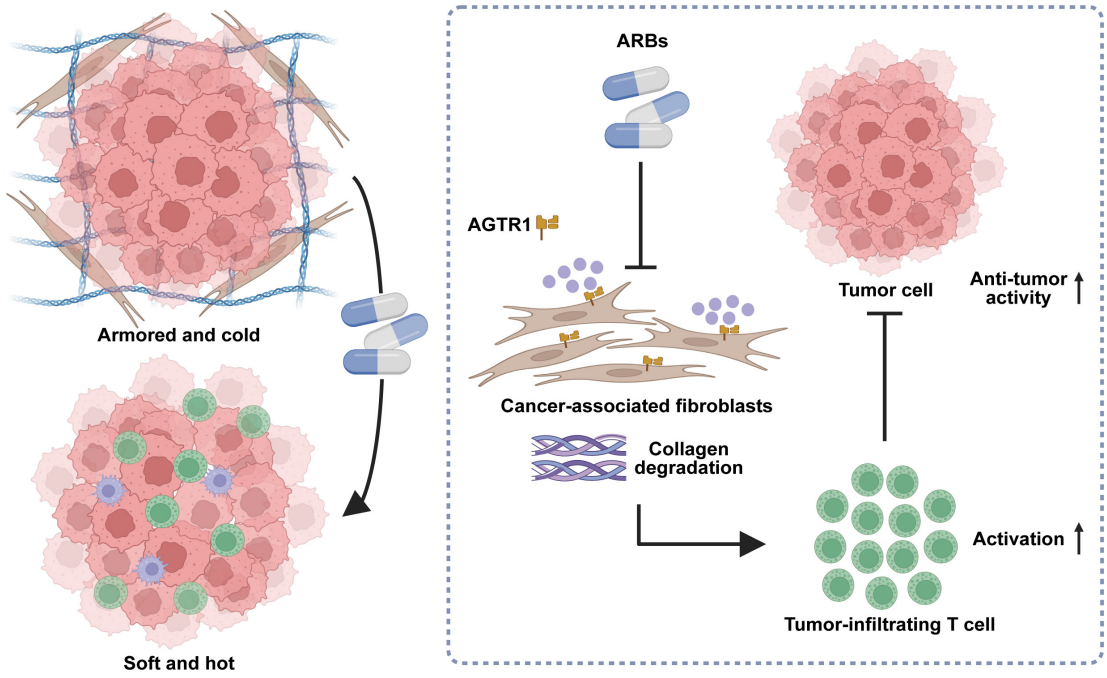

Figure 8 Schematic overview of the current study. Angiotensin receptor blocker (ARB) can make armored and cold tumors turn into soft and hot tumors, which greatly increases its therapeutic significance in clinical practice. Mechanistically, ARB targets AGTR1 and inhibits the RhoA/YAP axis to downregulate type I collagen expression. Ultimately, ARB promotes T cells activation and inhibits tumor immune escape. Created with BioRender.com.

YAP agonist XMU-MP-1 to restore losartan-mediated YAP inhibition, and the expression of type I collagen was notably enhanced. Overall, the AGTR1/RhoA/YAP axis is essential for type I collagen expression in CAFs, and inhibition of this pathway by ARB reverses the armored and cold status in solid tumors.

ACEI is another most used rennin–angiotensin system inhibitor. Due to similar mechanisms in lowering blood pressure, studies indiscriminately examine the role of the two drugs in immunotherapy outcomes.[14 63 64] However, the effects of these two drugs are diverse in tumor cells. As previously reported and revealed in our current study, ARB's drug target AGTR1 was highly expressed in CAFs and ARB inhibited the deposition of collagen I in the tumor tissues by suppressing CAFs.[51 53] As to ACEI, its drug target ACE could be detected in tumor cells in most cancer types according to protein expression data obtained from the Human Protein Atlas database,[45 46] suggesting ACEI could directly affect most tumor cells' biological behaviors. In addition, a population-based cohort reported that the use of ACEI was associated with an increased risk of lung cancer compared with the use of ARB.[65] It is biologically plausible that the use of ACEI resulted in the accumulation of bradykinin and substance P, which could promote the progression of lung cancer.[66 67] In addition to lung cancer, ACEI use was also associated with an increased risk of colorectal cancer.[68]

Although concerns about the long-term risk of cancer should be balanced against gains in life expectancy associated with the use of ACEI, the use of ACEI in special patients receiving ICB therapy should be particularly rediscussed. Medjebar *et al* reported that concurrent ACEI use statistically worsened prognosis due to that ACEI shapes an immunosuppressed TME state.[33] A retrospective study in 597 cases with multiple types of solid tumors exhibited that concomitant ACEI use was not associated with any improvement in objective response rate (ORR) in patients receiving ICB, which concomitant ARB use was associated with significantly improved ORR.[69] Similar findings were seen in a retrospective study presented at ESMO 2021 which focused on 127 patients with NSCLC receiving ICB therapy and showed that ARB use was related to an increase in ORR, in contrast to ACEI use was not associated with ORR improvement compared with patients receiving neither agent.[34] Thus, based on the above findings, we recommend that ARB should be selected as far as possible in patients who receive ICB therapy and also need antihypertensive therapy.

Although this study sheds light on the combination therapy of ARB and ICB for armored and cold tumors, several limitations warrant acknowledgment. First, the expression pattern of AGTR1 protein was only validated in several cancer types, leading to the conclusion that it was not completely compelling in all solid tumors. Thus, any conclusions in other cancer types beyond the current study need to be confirmed by further experiments. In addition, due to confounding factors in the cohort studies, although our conclusion of ARB sensitizing immunotherapy was based on meta-analysis, the sensitizing effect of ARB was still difficult to assess exactly. Last, whether ARB could be suitable for normotensive patients receiving ICB therapy was not mentioned in our research. However, a previous study reported that neoadjuvant therapy with FOLFIRINOX in combination with losartan followed by chemoradiotherapy in pancreatic cancer increased the R0

resection rate to 61%, and the blood pressure was tolerated in the dose range of 25–50 mg orally taken daily.[70] This study provides a safety reference for the application of ARB in the combination with ICB therapy in the general population. In addition, the $CD8^+$T cells were isolated from one healthy donor, which may lead to the potential selection bias. More studies on the regulation of tumor immunity by ARB need to be conducted.

CONCLUSIONS

In conclusion, we systematically screened potential concomitant medications based on our established immuno-collagenic subtypes and found that ARB is a promising candidate for armored and cold tumors. ARB inhibited type I collagen expression in CAFs via negatively regulating the RhoA/YAP axis, thus shaping an inflamed TME (figure 8). Overall, the current study provides a comprehensive rationale for the combination of ARB with ICB therapy in armored and cold tumors.

Author affiliations
[1]Department of Oncology, The First Affiliated Hospital of Nanjing Medical University, Nanjing, Jiangsu, China
[2]The First Clinical Medicine College, Nanjing Medical University, Nanjing, Jiangsu, China
[3]Department of Sports Medicine, Huashan Hospital Affiliated to Fudan University, Shanghai, China
[4]Departments of Endocrinology, The Affiliated Wuxi People's Hospital of Nanjing Medical University, Wuxi Medical Center, Nanjing Medical University, Wuxi, Jiangsu, China
[5]Department of Oncology, The Affiliated Wuxi People's Hospital of Nanjing Medical University, Wuxi Medical Center, Nanjing Medical University, Wuxi, Jiangsu, China
[6]Departments of Oncology, Xuzhou Central Hospital, The Xuzhou School of Clinical Medicine of Nanjing Medical University, Xuzhou, Jiangsu, China
[7]Departments of Gynecology, The Obstetrics and Gynecology Hospital Affiliated to Jiangnan University, Wuxi, Jiangsu, China
[8]Departments of Gynecology, Wuxi Maternal and Child Health Care Hospital, Nanjing Medical University, Wuxi, Jiangsu, China
[9]Departments of Gastroenterology, The Affiliated Wuxi People's Hospital of Nanjing Medical University, Wuxi Medical Center, Nanjing Medical University, Wuxi, Jiangsu, China
[10]Department of Physiology, School of Basic Medical Sciences, Nanjing Medical University, Nanjing, Jiangsu, China
[11]Department of Breast Surgery, The First Affiliated Hospital of Nanjing Medical University, Nanjing, Jiangsu, China
[12]Department of Central Laboratory, The First People's Hospital of Jintan, Jintan Affiliated Hospital of Jiangsu University, Changzhou, Jiangsu, China
[13]Collaborative Innovation Center for Cancer Personalized Medicine, Nanjing Medical University, Nanjing, Jiangsu, China

Correction notice This article has been corrected since it was first published to indicate that JM, JC, KY and ZL contributed equally.

Contributors YY, YC, YZhu, and JD conceived the study and participated in the study design, performance, coordination, and project supervision. JM and YC collected the public data and conducted the bioinformatics analysis. JM, KY, JY, JX, QZ, and JD collected the tumor samples and the clinical data. JM, JC, ZL, QL, YZhang, MW, and NX performed in vivo experiments and the tissues staining. JM, JC, KY, and ZL wrote the draft. YY and YZhu revised the manuscript. YY, YZhu, and JD received financial supports. All authors approved the final manuscript. YY is responsible for the overall content as the guarantor.

Funding This work was supported by the National Natural Science Foundation of China (82073194, 82272667), the High-level Innovation Team of Nanjing Medical University (JX102GSP201727), the Collaborative Innovation Center for Tumor Individualization Program (JX21817902/008), the Top Talent Support Program for Young and Middle-aged People of Wuxi Health Committee (BJ2023011, BJ2023075), the Project of Wuxi Medical Center of Nanjing Medical University (WMCC202319, WMCG202352), the Project of Jiangsu Province Health Committee (Z2023075), and Hengrui Pharmaceutical Clinical Research Fund of Personalized Medical Collaborative Innovation Center.

Competing interests None declared.

Patient consent for publication Not applicable.

Ethics approval Ethical approval for the use of TMAs was granted by the Clinical Research Ethics Committee in Outdo Biotech (No. SHYJS-CP-1910002, SHYJS-CP-1601008). Ethical approval for the collection of the immunotherapy cohort from The Affiliated Wuxi People's Hospital of Nanjing Medical University was granted by the Clinical Research Ethics Committee in The Affiliated Wuxi People's Hospital of Nanjing Medical University (No. KY23176). Ethical approval for the collection of the immunotherapy cohort from The First Affiliated Hospital of Nanjing Medical University was granted by the Clinical Research Ethics Committee in The First Affiliated Hospital of Nanjing Medical University (No. 2024-SR-017). All animal experiments were approved by the Laboratory Animal Ethics Committee at Nanjing Medical University (No. IACUC-2312041).

Provenance and peer review Not commissioned; externally peer reviewed.

Data availability statement Data are available on reasonable request.

Supplemental material This content has been supplied by the author(s). It has not been vetted by BMJ Publishing Group Limited (BMJ) and may not have been peer-reviewed. Any opinions or recommendations discussed are solely those of the author(s) and are not endorsed by BMJ. BMJ disclaims all liability and responsibility arising from any reliance placed on the content. Where the content includes any translated material, BMJ does not warrant the accuracy and reliability of the translations (including but not limited to local regulations, clinical guidelines, terminology, drug names and drug dosages), and is not responsible for any error and/or omissions arising from translation and adaptation or otherwise.

Open access This is an open access article distributed in accordance with the Creative Commons Attribution Non Commercial (CC BY-NC 4.0) license, which permits others to distribute, remix, adapt, build upon this work non-commercially, and license their derivative works on different terms, provided the original work is properly cited, appropriate credit is given, any changes made indicated, and the use is non-commercial. See http://creativecommons.org/licenses/by-nc/4.0/.

ORCID iDs
Jie Mei http://orcid.org/0000-0001-7799-8129
Yan Zhang http://orcid.org/0000-0002-7983-8396

REFERENCES

1 Ferrari N, Calvo F. Tumor microenvironment: unleashing metalloproteinases to induce a CAF phenotype. *Curr Biol* 2014;24:R1009–11.
2 Huang J, Zhang L, Wan D, *et al*. Extracellular matrix and its therapeutic potential for cancer treatment. *Signal Transduct Target Ther* 2021;6:153.
3 Yuan Z, Li Y, Zhang S, *et al*. Extracellular matrix remodeling in tumor progression and immune escape: from mechanisms to treatments. *Mol Cancer* 2023;22:48.
4 Laskowski TJ, Biederstädt A, Rezvani K. Natural killer cells in antitumour adoptive cell immunotherapy. *Nat Rev Cancer* 2022;22:557–75.
5 Byrne A, Savas P, Sant S, *et al*. Tissue-resident memory T cells in breast cancer control and immunotherapy responses. *Nat Rev Clin Oncol* 2020;17:341–8.
6 Hu Y, Hu Q, Li Y, *et al*. γδ T cells: origin and fate, subsets, diseases and immunotherapy. *Signal Transduct Target Ther* 2023;8:434.
7 Caligiuri G, Tuveson DA. Activated fibroblasts in cancer: Perspectives and challenges. *Cancer Cell* 2023;41:434–49.
8 Mao X, Xu J, Wang W, *et al*. Crosstalk between cancer-associated fibroblasts and immune cells in the tumor microenvironment: new findings and future perspectives. *Mol Cancer* 2021;20:131.
9 Mei J, Cai Y, Zhu H, *et al*. High B7-H3 expression with low PD-L1 expression identifies armored-cold tumors in triple-negative breast cancer. *NPJ Breast Cancer* 2024;10:11.
10 Mei J, Cai Y, Xu R, *et al*. Conserved immuno-collagenic subtypes predict response to immune checkpoint blockade. *Cancer Commun* 2024;44:554–75.
11 Fiala O, Buti S, Takeshita H, *et al*. Use of concomitant proton pump inhibitors, statins or metformin in patients treated with

pembrolizumab for metastatic urothelial carcinoma: data from the ARON-2 retrospective study. *Cancer Immunol Immunother* 2023;72:3665–82.
12 Edwards BK, Noone A-M, Mariotto AB, *et al*. Annual Report to the Nation on the status of cancer, 1975-2010, featuring prevalence of comorbidity and impact on survival among persons with lung, colorectal, breast, or prostate cancer. *Cancer* 2014;120:1290–314.
13 Magnuson A, Sattar S, Nightingale G, *et al*. A Practical Guide to Geriatric Syndromes in Older Adults With Cancer: A Focus on Falls, Cognition, Polypharmacy, and Depression. *Am Soc Clin Oncol Educ Book* 2019;39:e96–109.
14 Cortellini A, Tucci M, Adamo V, *et al*. Integrated analysis of concomitant medications and oncological outcomes from PD-1/PD-L1 checkpoint inhibitors in clinical practice. *J Immunother Cancer* 2020;8:e001361.
15 Mao W, Cai Y, Chen D, *et al*. Statin shapes inflamed tumor microenvironment and enhances immune checkpoint blockade in non-small cell lung cancer. *JCI Insight* 2022;7:e161940.
16 Pusztai L, Yau C, Wolf DM, *et al*. Durvalumab with olaparib and paclitaxel for high-risk HER2-negative stage II/III breast cancer: Results from the adaptively randomized I-SPY2 trial. *Cancer Cell* 2021;39:989–98.
17 Wolf DM, Yau C, Wulfkuhle J, *et al*. Redefining breast cancer subtypes to guide treatment prioritization and maximize response: Predictive biomarkers across 10 cancer therapies. *Cancer Cell* 2022;40:609–23.
18 Jung H, Kim HS, Kim JY, *et al*. DNA methylation loss promotes immune evasion of tumours with high mutation and copy number load. *Nat Commun* 2019;10:4278.
19 Mariathasan S, Turley SJ, Nickles D, *et al*. TGFβ attenuates tumour response to PD-L1 blockade by contributing to exclusion of T cells. *Nat New Biol* 2018;554:544–8.
20 Barretina J, Caponigro G, Stransky N, *et al*. The Cancer Cell Line Encyclopedia enables predictive modelling of anticancer drug sensitivity. *Nat New Biol* 2012;483:603–7.
21 Mei J, Cai Y, Chen L, *et al*. The heterogeneity of tumour immune microenvironment revealing the CRABP2/CD69 signature discriminates distinct clinical outcomes in breast cancer. *Br J Cancer* 2023;129:1645–57.
22 Butler A, Hoffman P, Smibert P, *et al*. Integrating single-cell transcriptomic data across different conditions, technologies, and species. *Nat Biotechnol* 2018;36:411–20.
23 Korsunsky I, Millard N, Fan J, *et al*. Fast, sensitive and accurate integration of single-cell data with Harmony. *Nat Methods* 2019;16:1289–96.
24 Wu T, Hu E, Xu S, *et al*. clusterProfiler 4.0: A universal enrichment tool for interpreting omics data. *Innovation (Camb)* 2021;2:100141.
25 The Gene Ontology Consortium. The Gene Ontology Resource: 20 years and still GOing strong. *Nucleic Acids Res* 2019;47:D330–8.
26 Shen Y, Wang X, Lu J, *et al*. Reduction of Liver Metastasis Stiffness Improves Response to Bevacizumab in Metastatic Colorectal Cancer. *Cancer Cell* 2020;37:800–17.
27 Cordenonsi M, Zanconato F, Azzolin L, *et al*. The Hippo transducer TAZ confers cancer stem cell-related traits on breast cancer cells. *Cell* 2011;147:759–72.
28 Wheeler SE, Shi H, Lin F, *et al*. Enhancement of head and neck squamous cell carcinoma proliferation, invasion, and metastasis by tumor-associated fibroblasts in preclinical models. *Head Neck* 2014;36:385–92.
29 Mei J, Liu Y, Yu X, *et al*. YWHAZ interacts with DAAM1 to promote cell migration in breast cancer. *Cell Death Discov* 2021;7:221.
30 Mei J, Yan T, Huang Y, *et al*. A *DAAM1* 3'-UTR SNP mutation regulates breast cancer metastasis through affecting miR-208a-5p-DAAM1-RhoA axis. *Cancer Cell Int* 2019;19:55.
31 Chiang C-H, Wang S-S, Chang Y-C, *et al*. The Effect of Renin–Angiotensin–Aldosterone System Inhibitors on Outcomes of Patients Treated with Immune Checkpoint Inhibitors: a Retrospective Cohort Study. *Clin Oncol* 2023;35:446–53.
32 Nuzzo PV, Adib E, Weise N, *et al*. Impact of renin-angiotensin system inhibitors on outcomes in patients with metastatic renal cell carcinoma treated with immune-checkpoint inhibitors. *Clin Genitourin Cancer* 2022;20:301–6.
33 Medjebar S, Truntzer C, Perrichet A, *et al*. Angiotensin-converting enzyme (ACE) inhibitor prescription affects non-small-cell lung cancer (NSCLC) patients response to PD-1/PD-L1 immune checkpoint blockers. *Oncoimmunology* 2020;9:1836766.
34 Pereira PM, Ferreira SC, Almodovar T. 969P Effect of angiotensin II inhibition on non-small cell lung cancer response to immune checkpoint blockers. *Ann Oncol* 2021;32:S835.
35 Xiong Y-X, Zhang X-C, Zhu J-H, *et al*. Collagen I-DDR1 signaling promotes hepatocellular carcinoma cell stemness via Hippo signaling repression. *Cell Death Differ* 2023;30:1648–65.
36 Sun M, Sun Y, Feng Z, *et al*. New insights into the Hippo/YAP pathway in idiopathic pulmonary fibrosis. *Pharmacol Res* 2021;169:105635.
37 Moon H, Cho K, Shin S, *et al*. High Risk of Hepatocellular Carcinoma Development in Fibrotic Liver: Role of the Hippo-YAP/TAZ Signaling Pathway. *Int J Mol Sci* 2019;20:581.
38 Mia MM, Singh MK. New Insights into Hippo/YAP Signaling in Fibrotic Diseases. *Cells* 2022;11:2065.
39 Koskina L, Andrikou I, Thomopoulos C, *et al*. Preexisting hypertension and cancer therapy: evidence, pathophysiology, and management recommendation. *J Hum Hypertens* 2023;37:331–7.
40 Lauder L, Mahfoud F, Azizi M, *et al*. Hypertension management in patients with cardiovascular comorbidities. *Eur Heart J* 2023;44:2066–77.
41 Busby J, McMenamin Ú, Spence A, *et al*. Angiotensin receptor blocker use and gastro-oesophageal cancer survival: a population-based cohort study. *Aliment Pharmacol Ther* 2018;47:279–88.
42 Zeman M, Skałba W, Wilk AM, *et al*. Impact of renin-angiotensin system inhibitors on the survival of patients with rectal cancer. *BMC Cancer* 2022;22:815.
43 Yang A, Wu H, Lau ESH, *et al*. Effects of RAS inhibitors on all-site cancers and mortality in the Hong Kong diabetes surveillance database (2002-2019). *EBioMedicine* 2022;83:104219.
44 Rhodes DR, Ateeq B, Cao Q, *et al*. AGTR1 overexpression defines a subset of breast cancer and confers sensitivity to losartan, an AGTR1 antagonist. *Proc Natl Acad Sci U S A* 2009;106:10284–9.
45 The human protein atlas. n.d. Available: https://www.proteinatlas.org/pathology
46 Uhlen M, Zhang C, Lee S, *et al*. A pathology atlas of the human cancer transcriptome. *Science* 2017;357:eaan2507.
47 Datta M, Chatterjee S, Perez EM, *et al*. Losartan controls immune checkpoint blocker-induced edema and improves survival in glioblastoma mouse models. *Proc Natl Acad Sci U S A* 2023;120:e2219199120.
48 Hashemzehi M, Rahmani F, Khoshakhlagh M, *et al*. Angiotensin receptor blocker Losartan inhibits tumor growth of colorectal cancer. *EXCLI J* 2021;20:506–21.
49 Takagi H, Kaji K, Nishimura N, *et al*. The Angiotensin II Receptor Blocker Losartan Sensitizes Human Liver Cancer Cells to Lenvatinib-Mediated Cytostatic and Angiostatic Effects. *Cells* 2021;10:575.
50 Li X, Luo X, Hu S. Modulating the tumor microenvironment improves antitumor effect of anti-PD-L1 mAb in breast cancer. *Bioimpacts* 2023;13:89–96.
51 Gu L, Zhu Y, Lee M, *et al*. Angiotensin II receptor inhibition ameliorates liver fibrosis and enhances hepatocellular carcinoma infiltration by effector T cells. *Proc Natl Acad Sci U S A* 2023;120:e2300706120.
52 AlQudah M, Hale TM, Czubryt MP. Targeting the renin-angiotensin-aldosterone system in fibrosis. *Matr Biol* 2020;91–92:92–108.
53 Diop-Frimpong B, Chauhan VP, Krane S, *et al*. Losartan inhibits collagen I synthesis and improves the distribution and efficacy of nanotherapeutics in tumors. *Proc Natl Acad Sci U S A* 2011;108:2909–14.
54 Pinter M, Jain RK. Targeting the renin-angiotensin system to improve cancer treatment: Implications for immunotherapy. *Sci Transl Med* 2017;9:eaan5616.
55 Mei J, Cai Y, Xu R, *et al*. Angiotensin-converting enzyme 2 identifies immuno-hot tumors suggesting angiotensin-(1-7) as a sensitizer for chemotherapy and immunotherapy in breast cancer. *Biol Proced Online* 2022;24:15.
56 Zhang T, Hu R, Wang Y, *et al*. Extracellular matrix stiffness mediates uterine repair via the Rap1a/ARHGAP35/RhoA/F-actin/YAP axis. *Cell Commun Signal* 2023;21:22.
57 Sakabe M, Thompson M, Chen N, *et al*. Inhibition of β1-AR/Gαs signaling promotes cardiomyocyte proliferation in juvenile mice through activation of RhoA-YAP axis. *Elife* 2022;11:e74576.
58 V H, Titus AS, Cowling RT, *et al*. Collagen receptor cross-talk determines α-smooth muscle actin-dependent collagen gene expression in angiotensin II–stimulated cardiac fibroblasts. *J Biol Chem* 2019;294:19723–39.
59 Chen Y, Zhao X, Sun J, *et al*. YAP1/Twist promotes fibroblast activation and lung fibrosis that conferred by miR-15a loss in IPF. *Cell Death Differ* 2019;26:1832–44.
60 Lu Z-N, Niu W-X, Zhang N, *et al*. Pantoprazole ameliorates liver fibrosis and suppresses hepatic stellate cell activation in bile duct ligation rats by promoting YAP degradation. *Acta Pharmacol Sin* 2021;42:1808–20.
61 Liu F, Lagares D, Choi KM, *et al*. Mechanosignaling through YAP and TAZ drives fibroblast activation and fibrosis. *Am J Physiol Lung Cell Mol Physiol* 2015;308:L344–57.
62 Piersma B, de Rond S, Werker PMN, *et al*. YAP1 Is a Driver of Myofibroblast Differentiation in Normal and Diseased Fibroblasts. *Am J Pathol* 2015;185:3326–37.

63 Kostine M, Mauric E, Tison A, *et al*. Baseline co-medications may alter the anti-tumoural effect of checkpoint inhibitors as well as the risk of immune-related adverse events. *Eur J Cancer* 2021;157:474–84.
64 Drobni ZD, Michielin O, Quinaglia T, *et al*. Renin-angiotensin-aldosterone system inhibitors and survival in patients with hypertension treated with immune checkpoint inhibitors. *Eur J Cancer* 2022;163:108–18.
65 Hicks BM, Filion KB, Yin H, *et al*. Angiotensin converting enzyme inhibitors and risk of lung cancer: population based cohort study. *BMJ* 2018;363:k4209.
66 Muñoz M, Pavon A. Long-term Use of Angiotensin-converting Enzyme Inhibitors Increases Substance P Levels, Which is Involved in the Risk of Lung Cancer. *Arch Bronconeumol* 2023;59:848–9.
67 Stewart JM. Bradykinin antagonists as anti-cancer agents. *Curr Pharm Des* 2003;9:2036–42.
68 Yarmolinsky J, Díez-Obrero V, Richardson TG, *et al*. Genetically proxied therapeutic inhibition of antihypertensive drug targets and risk of common cancers: A mendelian randomization analysis. *PLoS Med* 2022;19:e1003897.
69 Strauss J, Rajan A, Apolo A, *et al*. Impact of angiotensin II pathway inhibition on tumor response to anti PD(L)1 based therapy. *Eur J Cancer* 2020;138:S10.
70 Murphy JE, Wo JY, Ryan DP, *et al*. Total Neoadjuvant Therapy With FOLFIRINOX in Combination With Losartan Followed by Chemoradiotherapy for Locally Advanced Pancreatic Cancer. *JAMA Oncol* 2019;5:1020.